Scientific Reports

https://doi.org/10.1038/s41598-026-36677-x

Article in Press

Hidden patterns in volcanic seismicity: deep learning insights from Mt. Etna's 2020–2021 activity

Received: 9 July 2025

Accepted: 14 January 2026

Published online: 24 January 2026

Cite this article as: Abed W., Zali Z., Sciotto M. *et al.* Hidden patterns in volcanic seismicity: deep learning insights from Mt. Etna's 2020–2021 activity. *Sci Rep* (2026). https://doi.org/10.1038/s41598-026-36677-x

Waed Abed, Zahra Zali, Mariangela Sciotto, Ornella Cocina, Andrea Cannata, Matteo Picozzi, Patricia Martínez-Garzón, Alessandro Vuan, Angela Saraò & Monica Sugan

Hidden Patterns in Volcanic Seismicity: Deep Learning Insights from Mt. Etna's 2020–2021 Activity

Waed Abed[1], Zahra Zali[2], Mariangela Sciotto[3], Ornella Cocina[3], Andrea Cannata[3,4], Matteo Picozzi[1], Patricia Martínez-Garzón[2,5], Alessandro Vuan[1], Angela Saraò[1], Monica Sugan[1]

(1) National Institute of Oceanography and Applied Geophysics – OGS, Italy
(2) Helmholtz Centre Potsdam, German Research Centre for Geosciences – GFZ, Germany
(3) Istituto Nazionale di Geofisica e Vulcanologia - Osservatorio Etneo – INGV-OE, Italy
(4) Università di Catania, Dipartimento di Scienze Biologiche, Geologiche e Ambientali, Sezione di Scienze della Terra, Catania, Italy
(5) Rheinisch-Westfälische Technische Hochschule Aachen – RWTH University of Aachen, Germany

Corresponding author: wabed@ogs.it

Keywords: unsupervised machine learning, clustering, Etna, seismic regimes, preparatory phase, lava fountains

Abstract

Understanding the temporal evolution of volcanic activity is crucial for eruption forecasting and hazard assessment. We use an unsupervised machine learning method, Deep Embedded Clustering, to classify daily seismic spectrograms of Mount Etna between November 2020 and November 2021, a period that includes two major lava fountain sequences and quiescent phases. Using data from the horizontal components at two summit stations, we identify four clusters corresponding to distinct seismic regimes associated with different volcanic phases: (1) quiescence or non-dominant seismic features related to fluid dynamics, (2) fluid pressurisation indicated by elevated Long Period (LP) events, (3) preparatory phase, and (4) eruptive lava fountain episodes. These clusters closely match expert-defined volcanic phases and are validated against independent volcanic state indicators, including LP event catalogues, RMS amplitude trends, and eruption logs. Notably, a preparatory phase is observed before the lava fountains of February 2021, likely linked to the volcano's recharging phase. After the first eruptive sequence, a cluster dominated by LP events emerges, which may reflect fluid pressurisation within the volcanic system. The approach also identifies ambiguous days that reflect mixed behaviour. These results demonstrate the potential of unsupervised learning as a reliable and supportive tool for volcanic monitoring and eruption forecasting.

Introduction

Volcanic activity poses significant hazards to the population, critical infrastructure, and the environment. Accurate monitoring and forecasting of such phenomena are therefore essential for effective risk mitigation. Traditional volcano monitoring methods rely on multi-parametric observations, including seismicity, ground deformation, gas emissions, and visual inspections, which are typically analysed using manual or classical statistical methods [1,2]. While heavily instrumented volcanoes generate large volumes of high-resolution, multimodal data that challenge conventional analysis approaches, many observatories still operate with sparse monitoring

networks. Automatic classification tools offer a significant advantage in this context, providing stable, reproducible, and analyst-independent event classifications that support consistent, transparent, and reliable decision-making during volcanic unrest [3], and references therein.

In this context, machine learning (ML) methods have emerged as powerful tools for analysing complex, continuous, and high-dimensional geophysical datasets. ML techniques offer significant potential for improving the detection, classification, and forecasting of volcanic phenomena by recognising subtle patterns and non-linear relationships that may elude traditional methods. This applies to both well-instrumented, data-rich regions (e.g. [4]) and remote areas with limited instrumentation (e.g. [5]).

Both supervised and unsupervised ML techniques have proven effective in volcanic applications [6]. Supervised models trained on labelled datasets have successfully identified eruptions and classified seismic signals. Unsupervised approaches, such as clustering and dimensionality reduction, facilitate the integration of different features into coherent, multivariate representations of volcanic processes [7,8]. These integrative models not only reduce the uncertainties associated with monitoring individual parameters but also improve understanding of the complex, dynamic behaviour of active volcanoes. Key features include automatic detection of events (e.g. onset of a tremor or explosion), classification of sources (e.g. tectonic or volcanic), and forecasting of eruptions [9–17].

Mount Etna, the most active volcano in Europe, serves as a unique natural laboratory for the development and validation of unsupervised ML approaches, thanks to its persistent activity and robust, multi-parameter monitoring infrastructure. The Istituto Nazionale di Geofisica e Vulcanologia-Osservatorio Etneo (INGV-OE) operates a dense network of seismic, geodetic, and gas monitoring instruments around the volcano, providing high-resolution, long-term datasets. This network ensures optimal detection capability of the seismicity and precise hypocentral parameters across Etna [18,19].

Mount Etna exhibits a wide range of eruptive behaviours, predominantly centred at its summit craters, which frequently produce Strombolian explosions, lava fountains, and sustained lava effusion [20,21]. Unlike many volcanoes that undergo long periods of quiescence, Etna remains in a state of persistent unrest. Volcanic tremor and Long Period (LP) seismic events, sometimes collectively referred to in the literature as long period seismicity, are among the most intriguing and studied volcano-seismic signals recorded at volcanoes. Whether resulting from source or path effects, they are closely linked to magmatic and hydrothermal fluid dynamics and their interactions with volcanic structures, providing insight into volcanic processes ([22,23] and references therein) . At Mount Etna, these signals are regularly observed during both eruptive and non-eruptive periods, offering valuable insights into the volcano's internal processes as well as for monitoring purposes. In particular, the relationship between volcanic tremor and eruptive activity is well established, typically revealed through variations in amplitude, spectral content, and source location [24–28]. LP event analyses have contributed significantly to our understanding of Etna's shallow plumbing system, illuminating magma intrusions and pressurisation–depressurisation cycles within volcanic conduits (e.g., [25,27–30]).

For monitoring and surveillance purposes, INGV-OE developed automatic systems to early detect lava fountaining activities, based especially on volcanic tremor amplitude, infrasound, ground deformation data (tilt, GNSS, strain), SO2 flux, and thermal data (e.g. [31]). In addition to these parameters, the evaluation of the state of the volcano in the medium term relies on many parameters such as Volcano-tectonic (VT) seismicity occurrence (e.g. [32]), and other geophysical and geochemical evidence.

Machine learning applications at Etna are well established across various types of data and have expanded significantly in recent years. While non-seismic approaches have addressed lava flow mapping using satellite imagery [33], crystal chemistry and eruption intensity via clustering [34], and strain-based eruption characterisation [35], most advances have focused on seismic and acoustic data. ML has been used to classify seismo-volcanic events, detect unrest [8] and more recently to analyse volcanic tremor [36,37] and infrasound signals [38–40]. Notably, Watson [40] applied k-means clustering to infrasound to track eruptive evolution, while Nunnari [36] showed that tremor-based ML models could reliably distinguish between quiescent, Strombolian, and paroxysmal phases. More recently, Abazari et al. [41] demonstrated that deep neural networks applied to multi-sensor data significantly improve the discrimination of eruptive states at Etna, surpassing classical methods. The continuous seismic signal encompassing the Etna 2018 eruption was recently used as a case study, among others, to test a supervised deep learning-based method by Fee et al. [42], which uses spectrograms labelled from several volcanoes to detect and classify many types of volcano seismicity.

While supervised models have demonstrated high performance, it is worth remembering that they require extensive labelled data, a costly process that depends heavily on expert knowledge. In contrast, unsupervised methods offer scalable and potentially more generalisable approaches for seismic analysis, and are well suited to highlighting subtle, gradual, or previously unseen changes in seismicity, although their ability to detect subtle and continuous seismic variations still requires thorough validation.

In this study, we apply an unsupervised deep learning framework combining AutoencoderZ [4,43] and Deep Embedded Clustering [44–46] to daily seismic spectrograms recorded at two summit stations between November 2020 and November 2021, a period encompassing both quiescent phases and two major eruptive sequences. Our goal is to automatically identify clusters - groupings produced by the ML algorithm based on spectral similarities - and assess their correspondence with recognised volcanic phases. By comparing ML–derived clusters with independent volcanic indicators (lava fountains, VT and LP event catalogues, RMS amplitudes), we also evaluate the ability of unsupervised methods to detect hidden patterns and highlight diagnostic seismic transitions linked to subsurface processes such as magma ascent and gas accumulation. Our method integrates both single- and multi-station analyses to minimise spatial bias and improve the robustness of classification.

Data and Method

The data set analysed in this study covers the period from November 2020 to November 2021 and includes both quiet phases and two major cycles of lava fountains [47,48]. This temporal diversity provides an ideal context for evaluating the effectiveness of unsupervised ML in distinguishing between different phases of volcanic activity.

In this study, we analyse continuous seismic data recorded by the ECPN and ECNE stations, which are located near the summit craters of Mount Etna (Figure 1A) and do not exhibit significant site effects in the frequency bands relevant to our analysis [49]. In particular, the ECPN station is well suited for the detection of LP events and is used as a reference point for analysing volcanic tremor [28]. All analyses rely on horizontal components, as volcanic tremor signals are generally more pronounced on the horizontal plane [50]. The availability of waveform data for both stations is shown in Figure 1B.

To analyse the seismic data, we used Clustremor and AutoencoderZ (Text S1; Figure S1), unsupervised ML framework optimised for the analysis of seismic signals in a volcanic context [4,43]. Autoencoders are neural networks that perform feature extraction and dimensionality reduction by reconstructing the input data through

encoding and decoding steps [45,51]. The autoencoder architecture consists of: 1) Encoder that compresses the spectrogram input into a set of learnt features by using a series of convolutional layers and fully connected layers; 2) Bottleneck Layer - a narrow, central layer that forces the network to learn a low-dimensional representation of the data [52]; 3) Decoder that reconstructs the original input from the bottleneck features and verifies the effectiveness of the learnt representation. Convolutional layers in the encoder are connected to the corresponding transposed convolutional layers in the decoder through skip connection layers.

As shown in Figure 2, the workflow begins with the creation of daily spectrograms using the Short-Time Fourier Transform (STFT). Before this step, the signal was downsampled from 100 Hz to 18 Hz and a Butterworth-Bandpass filter between 0.5 and 8 Hz was applied. This frequency band includes the long period seismicity we are focused on and avoids dealing with higher frequency noise [42]. The STFT was applied using a sliding window to capture local frequency variations. Various window configurations were tested, and the most effective - corresponding to 25.8% overlap - was selected based on the performance of the optimal spectrogram visualisation. This configuration produced 2D spectrograms with dimensions of 1024 × 1024.

The spectrograms were input into the Encoder, which extracted K features through four convolutional layers, followed by a dense layer. These features were then used for the reconstruction of the input in the decoder. The Relative Bias (RB) metric was applied to determine the optimal value of K [53], defined as the configuration that minimises the difference between the original and reconstructed spectrograms. The extracted features were used for clustering using Deep Embedded Clustering (DEC), a technique that optimises feature learning and cluster assignment together [44–46]. This method facilitates the identification of seismic regimes by grouping similar feature patterns. To determine the optimal number of clusters, we analysed the Davies-Bouldin Index (DBI) [54] and the Calinski-Harabasz Index (CHI) [55]. For all stations and components, both metrics indicated that four clusters were optimal.

Finally, we visualised the clustering results using t-distributed Stochastic Neighbour Embedding (t-SNE), an unsupervised algorithm for mapping high-dimensional data into two dimensions [56,57]. To improve the interpretability of seismic variability over time, each cluster in Figure 2D is represented by a specific colour. Hereafter, the term *cluster* refers to the groupings produced by the ML algorithm, whereas *regime/phase* refers to their volcanological interpretation. The study began with a single-station analysis using data from the ECPN and ECNE stations. We then extended our investigation to a multi-station analysis.

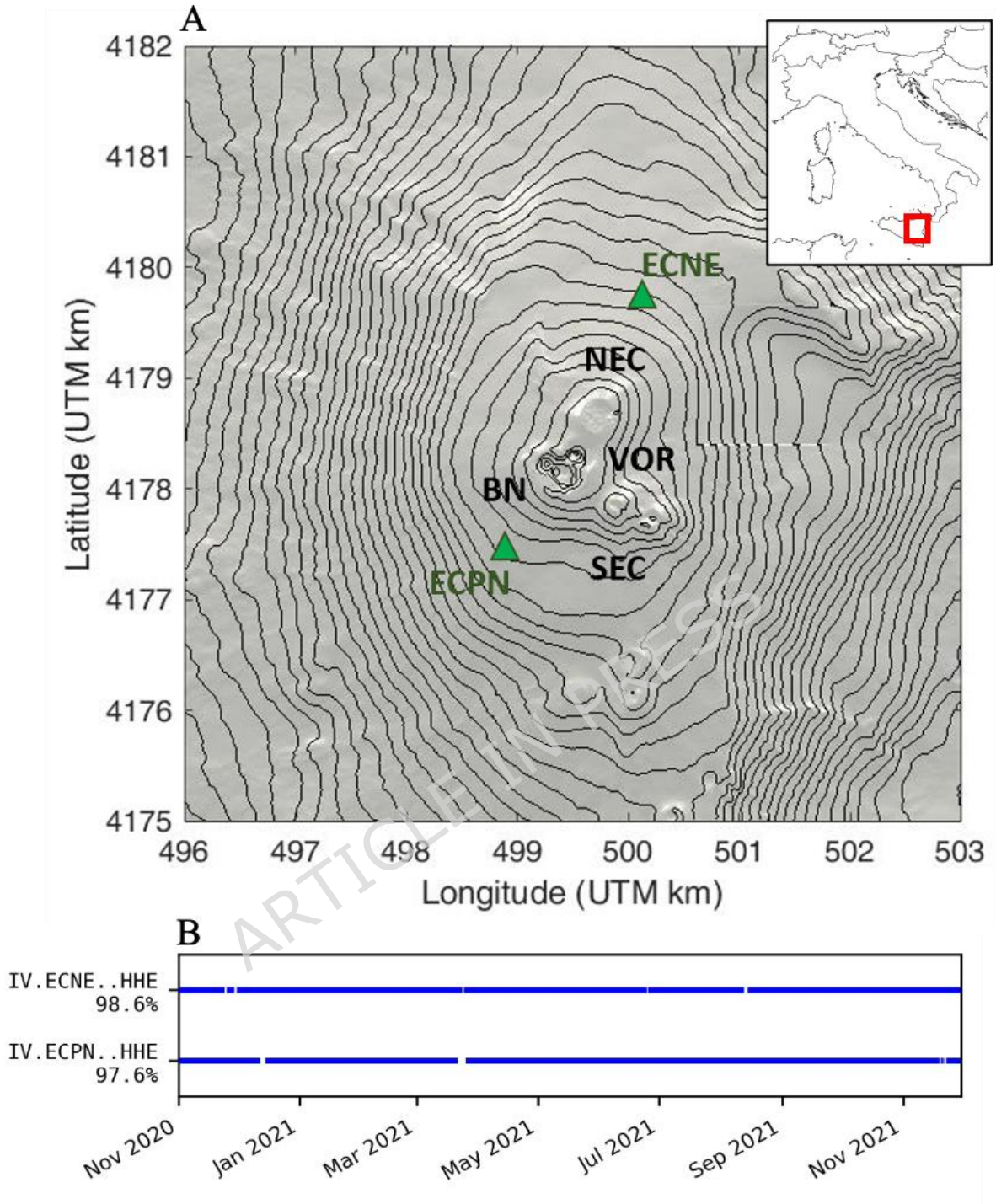

Figure 1: (**A)** Digital elevation model of the summit area of Etna [58], showing the locations of the ECPN and ECNE seismic stations and the summit craters (South-East Crater: SEC; Bocca Nuova: BN; Voragine: VOR; and North-East Crater: NEC). The inset map shows the location of Etna in southern Italy. **(B)** Seismic data availability from 1 November 2020 to 30 November 2021 (only the E component is shown).

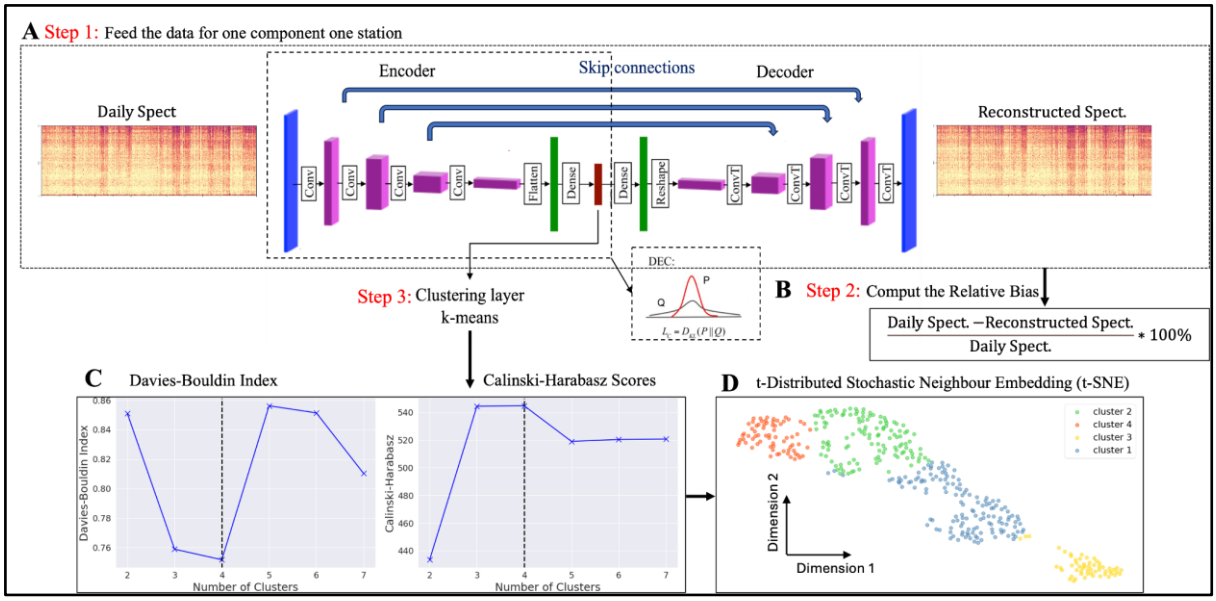

Figure 2. Overview of the workflow. The diagram shows the complete analytical pipeline using data from the ECPN-HHE component, where the lowest Relative Bias (RB) of 3.5% was achieved with 30 features. **(A)** Architecture of the AutoencoderZ model (adapted from Zali et al. [43]), showing feature extraction via the encoder and signal reconstruction via the decoder. **(B)** RB formula used to assess reconstruction accuracy and determine the optimal number of features for the bottleneck layer. **(C)** Determination of the number of clusters using the Davies-Bouldin and Calinski-Harabasz indices; dashed lines indicate the values corresponding to the optimal number of clusters. (**D**) Two-dimensional t-SNE visualisation of the clustering results; each point represents a single day of data, and colour indicates a different cluster.

Results and Discussion

Applying our workflow (Figure 2), we identified four clusters, retrospectively interpreted as corresponding to four distinct seismic regimes associated with the volcanic phases. These clusters were compared between stations and against independent volcanic state indicators (Figures 3 and 5) to validate their consistency, relevance, and interpretability.

Clustering results were first compared within each station across its two horizontal components to identify the dominant features driving classification. We then extended the analysis by assessing all stations and components together, merging them into a single dataset.

Independent volcanic state indicators

As independent volcanic state indicators, we used: i) the timing of lava fountain episodes [47], ii) the volcano-tectonic earthquake catalogue [59], iii) the Root Mean Square (RMS) amplitude, and iv) the LP events catalogue.

Lava fountains at Etna result from the rapid ascent of magma under high internal pressure, typically occurring at the summit craters; they are usually preceded by Strombolian activity [20,24]. During this study period, 62 intense lava fountain episodes were observed (Figure 3A). The eruptive phase studied here produced the most mafic magma observed in the last decade [47]. Three episodes occurred in December, and one episode in January 2021. Subsequently, two paroxysmal sequences occurred (16 February 2021–1 April 2021 and 19 May–23 October 2021; [60]). The median interval between lava fountain episodes was ~48 hours, while durations ranged from 9 to

629 minutes, with an average of ~92 minutes. Further statistical details are available in the supplementary material (Figure S2, Table S1).

Volcano-tectonic (VT) earthquakes [18] (Figure 3B) with epicentres within a 10 km radius of Etna's summit ($0.1 < M_L < 3.4$, Figure S3) and depths between -1.6 km a.s.l. and 28.9 km b.s.l. were also considered.

During the study period, several seismic swarms affected the volcanic area. A gradual increase in VT seismicity has been observed since late June 2020 [18,59,61], mainly affecting the shallow crust (depth < 3 km b.s.l.) in the central sector of the volcano. A remarkable variation in earthquake occurrence rate and energy release was observed on 31 December 2020 and 24 January 2021, when two seismic swarms occurred in the southwest (SW) and east (E) sectors of the volcano at intermediate and deep levels (10-20 km b.s.l.). Geochemical, petrological, ground deformation and seismological data indicated a significant episode of magma transfer from deep sources to the surface from December 2020 [60,61]. This trend continued until 13 February 2021, when a drastic reduction in shallow seismicity (depth <5 km) was observed, accompanying the lava fountain sequences from 16 February 2021. A renewal of deep VT seismicity occurred between April and May 2021 [19], preceding the onset of the second sequence of lava fountains.

The frequency band used in this study (0.5–8 Hz) is not well suited to fully capture signals associated with VT activity. Nevertheless, VT events [18] are presented together with other independent volcanic indicators to compare the identified cluster with the different processes occurring at Etna during the analysed period.

The RMS amplitude is a key indicator, as it primarily reflects variations in volcanic tremor amplitude often associated with changes in volcanic activity. The RMS amplitude time series (Figure 3C) was calculated on the vertical component of the signal acquired by the ECPN station. The seismic signal was first filtered in the 0.5–5 Hz frequency band and RMS amplitude values were computed over non-overlapping 10-second windows. To provide a robust, noise-resistant estimate of amplitude variation [28], for each 1-hour interval, the 25th percentile of these 10-second RMS values was calculated.

Based on RMS values, the INGV-OE "traffic light" system classifies volcanic tremor amplitude into three colour-coded levels, whose thresholds were recovered on roughly 15 years of ECPN RMS amplitude data: green-zone ($\leq 1.28 \times 10^{-6}$ m/s); yellow-zone (1.28×10^{-6} and 5.15×10^{-6} m/s), and red-zone ($> 5.15 \times 10^{-6}$ m/s). The yellow band represents the most commonly observed background activity, while green and red indicate anomalously low or high volcanic tremor amplitudes, respectively. These thresholds are station-specific and statistical in nature, and do not directly correspond to specific volcanic processes.

LP event catalogue consists of amplitude transients detected by four summit stations belonging to the INGV-OE permanent seismic network. Signals are filtered between 0.5–5.5 Hz, and an STA/LTA (short time average/long term average) trigger algorithm is implemented. The daily number of LP events (Figure 3D), was low during the first months of the investigated period, increasing after the first paroxysm sequence. It is important to note that the high volcanic tremor amplitude recorded during November 2020- February 2021 could have masked LP detections, which are triggered by STA/LTA-based methods. A sensitivity analysis of this aspect, however, was beyond the scope of the present study.

Single-station analysis

To identify common features and validate cluster stability, we compared the clustering results from stations ECPN and ECNE. Based on the DBI and CHI indices, four clusters were identified. Results from both stations are

presented in Figures 3E (ECPN) and 3F (ECNE), showing how the comparative analysis highlights the most energetic and consistent signals.

Table 1 summarises the description of each cluster in terms of days per station and independent volcanic state indicators (LP, RMS, and lava fountain occurrence). **Cluster 1** showed notable discrepancies in day-level assignments between stations, indicating variability in signal characteristics despite some shared days. **Cluster 2** emerged as one of the most dominant and consistent in terms of the number of assignments between stations, and appears associated with elevated LP seismic activity. **Cluster 3** corresponds to a well-defined temporal segment consistent between the two stations, characterised by high RMS amplitudes but relatively few LP events, possibly reflecting the masking of LP by elevated RMS. **Cluster 4** represents the best-aligned group in terms of assigned days, coinciding with the timing of lava fountain events. Finally, an "**Undefined**" category was used for days where the two horizontal components diverged in cluster assignment.

The clusters identified by the ML algorithm generally align with independent volcanic indicators (Figure 3) across both horizontal components. Figure 4 presents examples of daily spectrograms and corresponding waveforms for the four clusters identified by the unsupervised ML analysis. Cluster 1 predominantly shows weak, diffuse energy across a broad frequency range, and contemporaneously low activity is observed representing except for occasional Strombolian explosions preceding paroxysms. It is characterised by RMS values ranging from green to red-zone, and great variability between stations, and low to moderate LP event rates. Cluster 2 is defined by low overall energy punctuated by short-duration, transient events, appearing as thin, vertical streaks concentrated in the 0.5–8 Hz range, interpreted as LP events associated with fluid dynamics within the shallower portion of the plumbing system. Cluster 3 is marked by persistent, high-amplitude volcanic tremor with dominant energy between 0.5 and 5 Hz, indicative of sustained pressurisation of the volcano and heightened volcanic activity. Cluster 4 clearly captures lava fountain episodes, displaying intense broadband energy and characteristic harmonic tremor, a signature of vigorous magma ascent and degassing during paroxysmal activity.

Our clustering results align well with those from independent volcanic state indicators (e.g., RMS amplitude, LP event occurrence rates). However, the unsupervised clustering approach processes the entire spectral content of the data, capturing subtle patterns that may not be fully represented by individual parameters. While the clusters correlate with known eruptive phases, the model's strength lies in its ability to synthesise complex, multivariate relationships within the spectrograms and may offer insights beyond conventional threshold-based analyses.

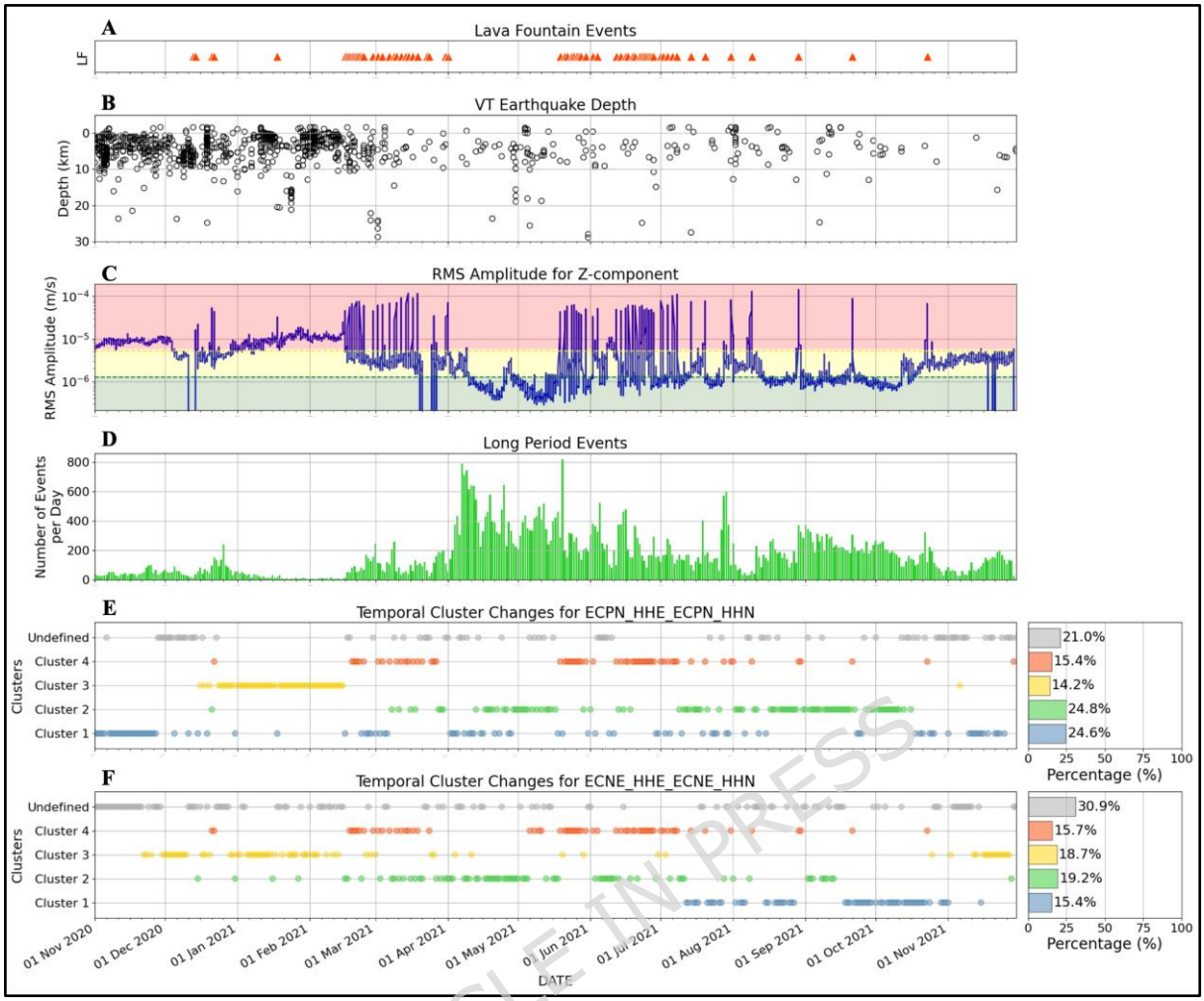

Figure 3: Temporal evolution of clusters in relation to independent volcanic state indicators. (A) Occurrence of lava fountain events during the study period, based on data from Giuffrida et al. [47] and Proietti et al. [48]. (B) Depth of volcano-tectonic earthquakes (VT) over time, recorded within a 10 km radius of Mt Etna's summit. (C) Daily mean Root Mean Square (RMS) amplitude for the ECPN seismic station (Z component). (D) Daily count of Long Period events. (E) and (F) show the temporal distribution of clusters identified by AutoencoderZ for the ECPN and ECNE stations, respectively, across both horizontal components. An Undefined category was assigned to days when the two horizontal components yielded different cluster assignments. The panels on the right show the percentage of days that each cluster represents with respect to the entire analysed period.

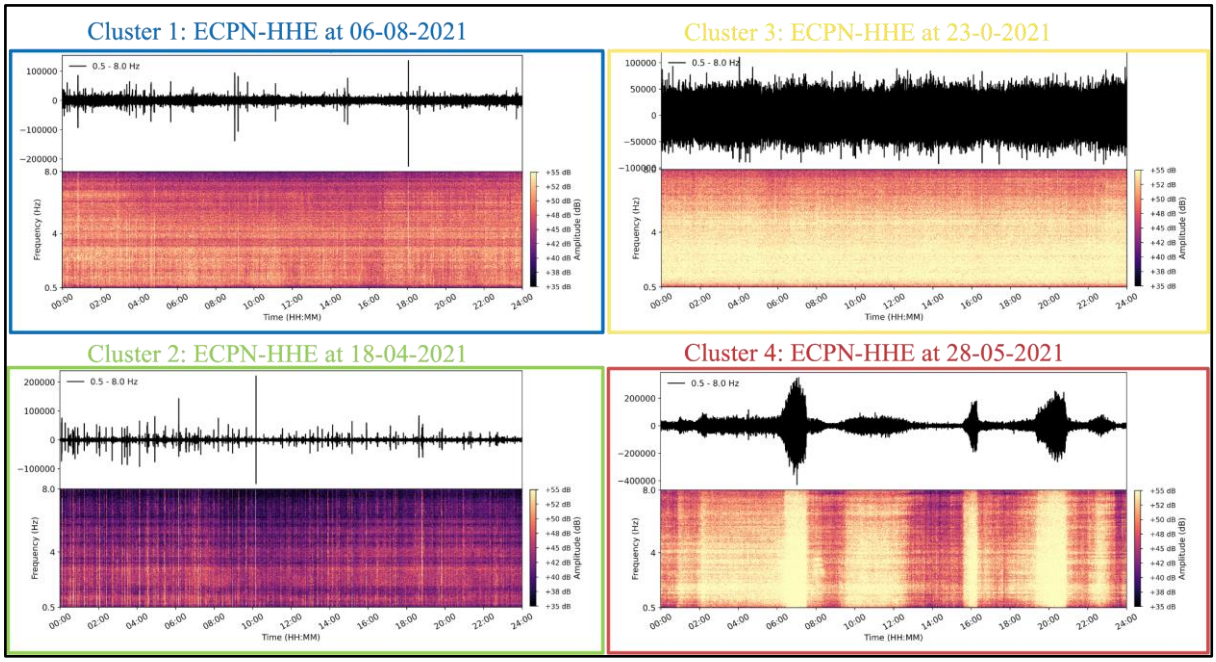

Figure 4: Examples of daily spectrograms and corresponding seismic waveforms for representative days from each of the four clusters identified by the unsupervised ML algorithm. Cluster 1 includes quiescent periods and displays weak, broadband energy without a dominant spectral feature. Cluster 2 is characterised by LP events, appearing as vertical bands of energy concentrated in the 0.5–8 Hz range. Cluster 3 shows persistent, high-amplitude tremor with sustained energy in the 0.5–5 Hz band. Cluster 4 corresponds to lava fountain episodes and exhibits classic features of explosive paroxysms, including harmonic tremor and broadband energy bursts.

Table 1: Cluster-Wise Frequency Distribution of Volcanic Activity Conditions for each Station and Cluster.

Station	Class	Total Days	Lava Fountain Days*	Lava Fountain Day %	Days > 200 LP	Days > 200 LP %	RMS Red Days	RMS Red Days %
ECPN	Cluster 1	97	3	3.1%	24	24.7%	33	34.0%
	Cluster 2	98	1	1.0%	55	56.1%	1	1.0%
	Cluster 3	56	0	0%	1	1.8%	47	83.9%
	Cluster 4	61	50	82%	21	34.4%	44	72.1%
	Undefined	82	11	13.4%	21	25.6%	18	22%
ECNE	Cluster 1	61	0	0%	14	23%	0	0%
	Cluster 2	76	6	7.9%	46	60.5%	13	17.1%
	Cluster 3	74	0	0%	5	6.8%	38	51.4%
	Cluster 4	62	55	88.7%	23	37.1%	48	77.4%
	Undefined	122	4	3.3%	34	27.9%	44	36.1%

*Lava fountain days in the references (Giuffrida et al. [47] and Proietti et al. [48]) total 65 days; 3 days are missing from ECPN, while 3 days are missing from ECNE. The values represent the percentage of days in each cluster associated with a given condition, calculated as $p_{ij} = \frac{N_{ij}}{N_i}$ where p_{ij} is the percentage of days in cluster *i* corresponding to condition *j*, N_{ij} is the number of days in cluster *i* exhibiting condition *j*, and N_i is the total number of days in cluster *i*. A threshold of 200 LP events per day

(70th percentile) was used to classify days with elevated LP activity. Note that the total number of days is 395; ECPN provides data for 389 of the days, while ECNE provides data for 391 days.

Multi-station analysis

To strengthen our analysis, we merged data from the horizontal components of the two seismic stations. For this purpose, we developed a filter to identify, for each day, the cluster label most frequently assigned across components. Based on the number of horizontal components assigned to the same cluster by the algorithm, we defined three configurations (Figure 5). Configuration A (Config A) includes days when at least two components agree, regardless of the station. Configuration B (Config B) refers to days when three components agree (for example, both components from one station and one from the other). Configuration C (Config C) corresponds to days when all four components, both from ECPN and ECNE, concur on the dominant cluster label. To quantitatively determine the interpretability of clustering in terms of volcanic state, we computed the relative frequency (as a percentage) of three key conditions within each cluster identified by the algorithm: lava fountain occurrence, LP event counts exceeding 200 per day (a threshold corresponding to the 70th percentile of daily LP counts in our dataset; see Figure S4), and RMS amplitude in the red zone. These results are reported in Table 2.

Cluster 1 does not show well-defined temporal sequences but instead appears scattered across the observation period, with only two intervals of partial coherence between configurations: 1) November 2020, characterised by high RMS amplitude (corresponding to the red-zone), relatively high VT seismicity, and low LP event rates; 2) October 2021, featuring medium RMS amplitude (corresponding to the yellow-zone) and moderate LP activity (on average between 100 and 200 events per day). In Config C, Cluster 1 accounted for only 3.3% of the dataset, with occurrences mainly concentrated between July and November 2021. Associated volcanic state indicators show low to moderate LP events and variable RMS amplitude (see Figures 3C and 3D). RMS exceeded the red-zone threshold on 36.6% (Config A) and 36.1% (Config B) of Cluster 1 days, but was absent in Config C. Only 23.1% of Cluster 1 days exceeded the 200 LP-event per day threshold (Table 2).

The inconsistent presence across configurations suggests this cluster is not characterised by a dominant or coherent seismic feature. Volcanic activity in this period is represented by occasional Strombolian explosions.

Cluster 2 exhibited strong temporal coherence across all configurations, spanning a sustained period from 8 March to 13 September 2021, with peak activity between May and early June (Figure 5). This cluster was most prominent in Config A (21%) and Config B (14.4%), while Config C identified a more selective subset (7.8%).

The cluster is distinctly associated with an elevated LP occurrence rate (Figure 5A–C). In Configs A and B, approximately 70% of Cluster 2 days recorded more than 200 LP events (Table 2). Lava fountains and high RMS amplitudes were rare in this cluster, particularly in Config C, which captured the clearest representation of LP event-dominant behaviour.

Cluster 3 emerged as a well-defined temporal segment across all configurations, beginning on 30 November 2020 in Configs A and B, and on 18 December 2020 in Config C. All three configurations converged on an end date in mid-February 2021. This cluster is associated with: 1) increasing high RMS amplitude (69.4% of Cluster 3 days in Config A and B; 93.8% in Config C, as shown in Figure 5D and Table 2), 2) increased VT seismicity within a 10 km radius from the summit area, and 3) a very low frequency of daily LP events (on average, less than ~50

events per day; see Figures 3B, 3C, and 3D). In November 2021, another group of days appeared in Cluster 3 for Config A and B. This period was marked by medium RMS amplitude and a noticeable trend of increasing daily LP events, but still below the threshold of 200 LP events per day. Closer inspection of seismic waveforms and spectrograms from 30 November 2020 to 16 February 2021 (Configs A and B) revealed a phase between 5 and 20 December, characterised by mixed or unstable spectral features (Figure 5D, dashed square). After this period, the signal evolved into sustained tremor, potentially representing a precursory phase to the eruptive activity period classified under Cluster 4 (Figure 5D, solid square).

Cluster 4 showed strong agreement across all configurations and was temporally confined to two well-defined time windows: 1) 18 February to 19–24 March 2021 (depending on configuration); 2) 6–19 May to 23 October 2021 (with a staggered start but a uniform end date). Cluster 4 was consistently and strongly associated with lava fountaining (see Figure 3A), observed on 88.5% (Config A), 88.3% (Config B), and 94.3% (Config C) of Cluster 4 days. High RMS amplitude (see Figure 3C) occurred on 77%, 78.3%, and 83% of Cluster 4 days in Configs A, B, and C, respectively (Figure 5A–C, Table 2). These high correlations confirm Cluster 4 as the most volcanologically diagnostic, reflecting periods of paroxysmal eruptive behaviour.

The **Undefined** cluster includes days with inconsistent cluster assignments across components. As expected, its prevalence increases with the strictness of the agreement criterion: 27.3% in Config A, 36.7% in Config B, and 67.3% in Config C.

This cluster likely represents ambiguous or mixed seismic behaviour, possibly resulting from variability in signal type and strength across stations, differences in site sensitivity or proximity to source regions, or overlapping volcanic processes that do not dominate the spectral signature.

In Config C, 29.3% of Undefined days showed high LP counts, and 26% exhibited elevated RMS amplitude, suggesting complex, non-exclusive features that defy clear categorisation.

The persistence of an Undefined cluster, particularly in configurations requiring strict component agreement, highlights ongoing challenges in classifying mixed or ambiguous signals. These periods may coincide with hybrid processes (e.g., overlapping tremor, tectonic earthquakes, and LP events), which resist straightforward categorisation.

Our analysis identified four clusters, each aligning with known volcanic regimes (Table S2). While unsupervised ML excels at pattern recognition, the physical interpretation of these clusters remains contingent on integrating complementary datasets, such as gas flux measurements, thermal imagery, or ground deformation records.

Misclassifications and limitations

Our analyses highlight that the clustering algorithm occasionally misidentified events with lava fountains, i.e., Cluster 4 (see Tables S3 and S4). Furthermore, some days - three days based on Config C and seven days based on Configs A and B - were incorrectly classified as eruptive despite no confirmed surface activity. This was often due to missing hourly data (for example, 29 November 2021), increased LP activity, or short-lived tremor bursts occurring close in time to confirmed eruptive episodes. Short-lasting episodes of increased volcanic tremor may also have contributed to this misclassification (e.g. 23 May, 7 July and 30 August). The algorithm detected early signs of the second eruptive cycle up to three days in advance, likely because LP occurrence rate exceeded the 93rd percentile of daily LP counts in our dataset (see Figure S4); extending the catalogue over a longer time span

would allow for a more robust threshold. Conversely, 15 actual lava fountain days were not assigned to Cluster 4. Reasons include events of short duration (e.g. 21 December 2020, 16 February 2021), late evening onset causing peak activity to extend beyond the observation window (e.g. 17 February, 9 March), Strombolian activity precursors turning into lava fountains and blurring event boundaries, and significant data loss (over 7 hours) on four of these days. Furthermore, in Andronico et al. [20], the eruptive style of episodes occurred on 13, 14 and 21 December 2020 and 18 January 2021 were classified as "transitional activity" rather than lava fountains, meaning strong Strombolian activity alternating with short periods of lava fountains.

VT earthquakes were also detected during the outlier days, possibly obscuring or distorting volcanic tremor signals. The simultaneous presence of multiple seismic signals within a time interval can contribute to difficulties in successful classification. These results emphasise the importance of considering temporal dynamics, multiphase activity, and data completeness when interpreting unsupervised classifications.

Moreover, expanding beyond the current two summit stations could enhance resolution and allow testing of robustness under different network geometries. Methodological refinements, such as adjusting spectrogram resolution, frequency band selection, or the dimensionality reduction strategy, could further stabilise clustering outcomes and improve feature extraction. Finally, integrating independent indicators will strengthen their volcanological meaning and broaden the applicability of our results.

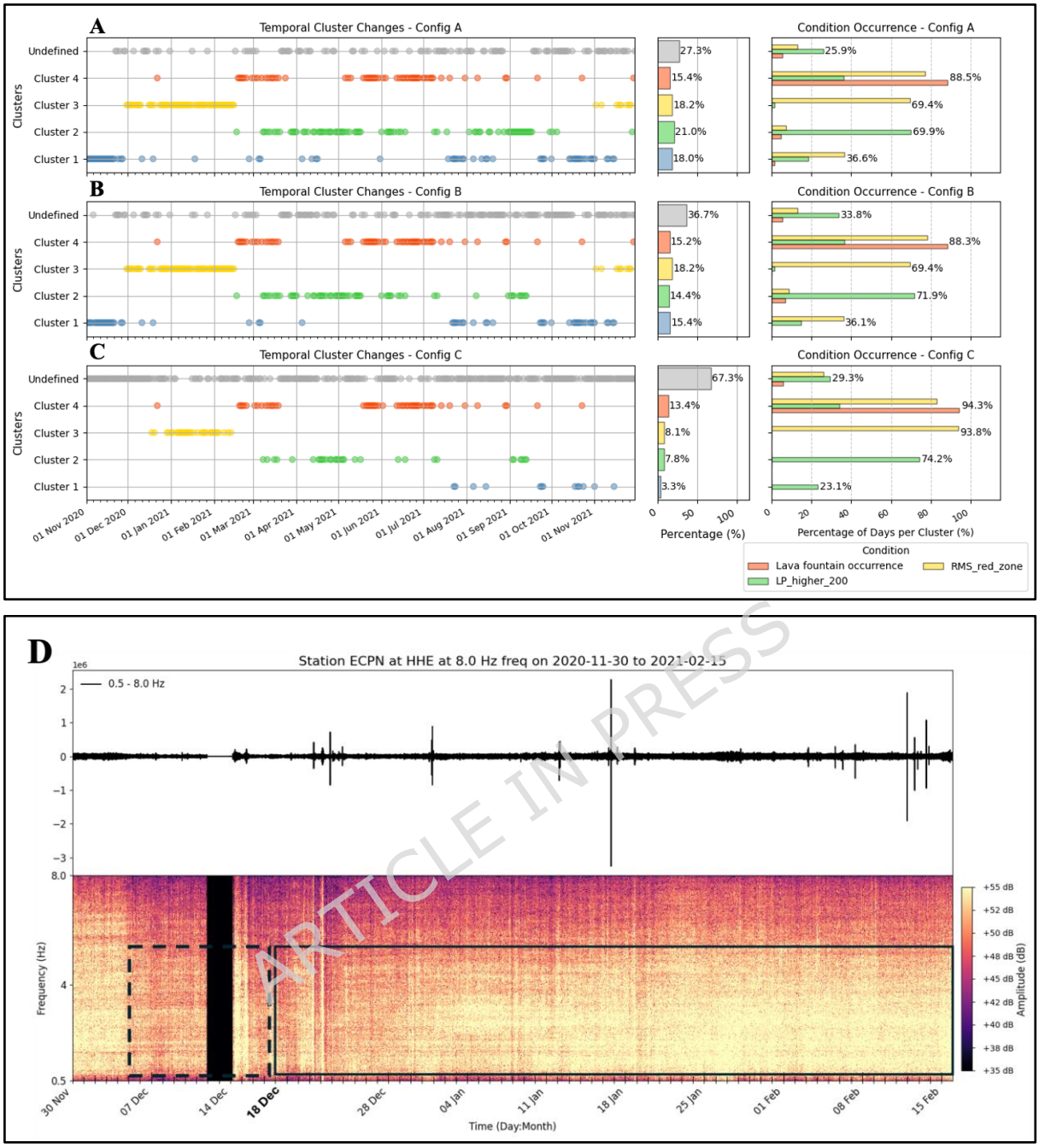

Figure 5: Temporal evolution of clusters in relation to independent volcanic state indicators. Panels (A), (B), and (C) show different configurations of seismic station combinations used for clustering. In each row, the left plot shows the temporal distribution of cluster assignments over the analysis period, with each dot representing a day; the centre plot displays the proportion of time each cluster was active during the analysed period; and the right plot presents the relative frequency of specific volcanic-related conditions based on independent observations, such as the presence of lava fountains, elevated RMS amplitude in the red-zone, and high LP event rates (more than 200 events per day) for each cluster, with only the dominant condition annotated (details are provided in Table 2). Part (D) provides a spectrogram and waveform for Cluster 3 based on the starting day for Config A and B up to mid-February. The dashed square marks mixing signals, while the solid black square marks the continuous signals and the change in amplitude based on the starting day as assigned by Config C. The data for this spectrogram were taken from ECPN using the eastern component. Missing data are shown in black on the spectrogram.

Table 2: Cluster-Wise Frequency Distribution of Volcanic Activity Conditions for each Multi-station configuration.

CONFIG	CLASS	TOTAL DAYS	LAVA FOUNTAIN DAYS*	LAVA FOUNTAIN DAY %	DAYS > 200 LP	DAYS > 200 LP %	RMS RED DAYS	RMS RED DAYS %
CONFIG A	Cluster 1	71	1	1.4%	13	18.3%	26	36.6%
	Cluster 2	83	4	4.8%	58	69.9%	6	7.2%
	Cluster 3	72	0	0%	1	1.4%	50	69.4%
	Cluster 4	61	54	88.5%	22	36.1%	47	77%
	Undefined	108	6	5.5%	28	25.9%	14	13%
CONFIG B	Cluster 1	61	0	0%	9	14.7%	22	36.1%
	Cluster 2	57	4	7%	41	71.9%	5	8.8%
	Cluster 3	72	0	0%	1	1.4%	50	69.4%
	Cluster 4	60	53	88.3%	22	36.7%	47	78.3%
	Undefined	145	8	5.5%	49	33.8%	19	13.1%
CONFIG C	Cluster 1	13	0	0%	3	23.1%	0	0%
	Cluster 2	31	0	0%	23	74.2%	0	0%
	Cluster 3	32	0	0%	0	0%	30	93.8%
	Cluster 4	53	50	94.3%	18	33.9%	44	83%
	Undefined	266	15	5.6%	78	29.3%	69	26%

*Lava fountain days in the references (Giuffrida et al. [47] and Proietti et al. [48]) total 65 days; 3 days are missing from ECPN, while 3 days are missing from ECNE. More details found in Table S3 and Table S4. See Table 1 for details.

Conclusion

This study demonstrates that unsupervised ML, when applied to high-resolution seismic data, can effectively disentangle complex volcanic processes and isolate preparatory eruption signals (i.e., Cluster 3 in the analysed period). By bridging the gap between raw seismic data and interpretable phases of volcanic activity, our approach offers an alternative that enables observatories to respond to evolving unrest phases.

Using AutoencoderZ and DEC, we analysed seismic data from two stations recorded between 1 November 2020 and 30 November 2021. We identified four different clusters corresponding to recognised volcanic regimes: (1)

quiescence or non-dominant seismic features related to fluid dynamics, (2) Long Period (LP) event-dominated fluid pressurisation, (3) preparatory phase, and (4) lava fountains episodes. These clusters closely align with expert classifications and achieve high temporal resolution, showing the ability of unsupervised ML to capture dominant spectral signatures and subtle transitions in volcanic activity.

A key result is the identification of a preparatory phase (Cluster 3) from mid-December 2020 to mid-February 2021, characterised by increasing tremor amplitudes preceding the lava fountains occurring from 16 February onwards in the first eruptive sequence, likely linked to the volcano recharging phase. The subsequent emergence of an LP event-dominated phase (Cluster 2) and the resumption of deep VT seismicity from April 2021 suggest ongoing volcanic activity and a new recharge phase prior to the second eruptive sequence.

Notably, in certain configurations (A and B), a preparatory regime was detected at the end of November 2021, potentially linked to the eruptive activity that occurred shortly thereafter. However, a new analysis extending the temporal coverage of the dataset beyond November 2021 will be required to validate this interpretation.

Importantly, the ML approach captures complex spectral patterns across multiple stations and components, providing insights that complement traditional amplitude-based metrics and highlighting hybrid behaviours and subtle transitions that are often overlooked in conventional analyses. The high predictive accuracy (~95%) of Cluster 4 in identifying eruption days emphasises its potential as a robust indicator for operational environments.

From an operational perspective, our clustering framework should be viewed as complementary to the multiparametric monitoring system operated by INGV-OE. While the current implementation, based on daily windows, is not real-time, it highlights consistent patterns of precursory seismicity that can support interpretation during unrest. Indeed, in the context of medium-term volcanic activity assessment, identifying a preparatory regime (Cluster 3) gains value when combined with independent indicators, as it groups together seismic signals reflecting magma and fluid migration towards the surface.

A promising avenue for future work is to extend the approach to higher temporal resolutions (less than daily scale, e.g., 6–8 hours with overlap), enabling the detection of short-lived or transient spectral features. Expanding the analysis to radial and tangential components could also improve consistency across stations. Nonetheless, ambiguities in smaller events highlight the need for expert review, especially in noise-sensitive or low-activity environments. These results also emphasise the challenge of interpreting ML-based precursors in volcanic settings. Hybrid approaches that integrate unsupervised clustering with supervised classifiers could enable improved predictions in poorly supervised regions.

Finally, while unsupervised ML effectively captures complex spectro-temporal patterns, its full potential is realised when combined with multidisciplinary observations, including gas emissions, thermal imagery, and ground deformation, to translate data-driven insights into actionable information for volcanic risk mitigation. Together, these advances pave the way for more robust and timely eruption forecasting and a deeper understanding of volcanic dynamics.

Acknowledgements

Computations are performed at CINECA in the framework of the HPC-TRES program agreement between OGS and CINECA.

Author contributions

M.Su. designed the study. W.A. and Z.Z. performed machine learning modelling and W. A., Z.Z. and M.Su. analysed the results. W.A. prepared the data for the analysis. M.S., O. C. and A.C. provided the dataset of Long Periods events, RMS amplitude values and earthquake catalogue.

The first manuscript draft was written by W.A., M.Su. and A.S. All the authors contributed to the evaluation and discussion of the results and the writing of the final manuscript.

Funding

This study was carried out within the RETURN Extended Partnership and received funding from the European Union Next-GenerationEU (National Recovery and Resilience Plan – NRRP, Mission 4, Component 2, Investment 1.3 – D.D. 1243 2/8/2022, PE0000005). Z.Z. and P.M.G acknowledge funding from the European Research Council (ERC) under the European Union's Horizon 2020 research and innovation program (Grant 101076119 for project QUAKEHUNTER). In addition, this study was supported by funding provided by the Italian Presidenza del Consiglio dei Ministri—Dipartimento della Protezione Civile (DPC). This paper does not necessarily represent DPC official opinion and policies.

Competing interests

The authors declare no competing interests.

Additional information

Supplementary information: Text S1, Figure S1, Figure S2, Figure S3, Figure S4, Table S1, Table S2, Table S3.

Data Availability Statement

Seismic waveforms used in this study (ECPN, ECNE stations) were recorded by the INGV-OE permanent network and are available on the EIDA seismic archive, https://eida.ingv.it/en/getdata. The VT catalogue is publicly available at https://www.ct.ingv.it/; the LP catalogue and RMS values can be provided upon request.

All other relevant data are included in the article and its Supplementary Information.

Code availability

The code related to AutoencoderZ and DEC are freely available at https://github.com/ZahraZali/AutoencoderZ.

References

1. McNutt, S. R. Seismic Monitoring and Eruption Forecasting of Volcanoes: A Review of the State-of-the-Art and Case Histories. in *Monitoring and Mitigation of Volcano Hazards* 99–146 (Springer Berlin Heidelberg, Berlin, Heidelberg, 1996). doi:10.1007/978-3-642-80087-0_3.
2. White, R. A. & McCausland, W. A. A process-based model of pre-eruption seismicity patterns and its use for eruption forecasting at dormant stratovolcanoes. *J. Volcanol. Geotherm. Res.* **382**, 267–297 (2019).
3. Lowenstern, J. B. *et al.* Guidelines for volcano-observatory operations during crises: recommendations from the 2019 volcano observatory best practices meeting. *J. Appl. Volcanol.* **11**, 3 (2022).
4. Zali, Z., Mousavi, S. M., Ohrnberger, M., Eibl, E. P. S. & Cotton, F. Tremor clustering reveals pre-eruptive signals and evolution of the 2021 Geldingadalir eruption of the Fagradalsfjall Fires, Iceland. *Commun. Earth Environ.* **5**, 1 (2024).
5. Cesca, S. *et al.* Massive earthquake swarm driven by magmatic intrusion at the Bransfield Strait, Antarctica. *Commun. Earth Environ.* **3**, 89 (2022).
6. Carniel, R. & Guzmán, S. R. Machine Learning in Volcanology: A Review. in *Updates in Volcanology - Transdisciplinary Nature of Volcano Science* (ed. Németh, K.) (IntechOpen, 2021). doi:10.5772/intechopen.94217.
7. Brancato, A., Buscema, P. M., Massini, G. & Gresta, S. Pattern Recognition for Flank Eruption Forecasting: An Application at Mount Etna Volcano (Sicily, Italy). *Open J. Geol.* **06**, 583–597 (2016).
8. Messina, A. & Langer, H. Pattern recognition of volcanic tremor data on Mt. Etna (Italy) with KKAnalysis—A software program for unsupervised classification. *Comput. Geosci.* **37**, 953–961 (2011).
9. Corradino, C., Amato, E., Torrisi, F., Calvari, S. & Del Negro, C. Classifying Major Explosions and Paroxysms at Stromboli Volcano (Italy) from Space. *Remote Sens.* **13**, 4080 (2021).
10. Falsaperla, S., Graziani, S., Nunnari, G. & Spampinato, S. Automatic classification of volcanic earthquakes by using Multi-Layered neural networks. *Nat. Hazards* **13**, (1996).
11. Fernando, L., Román, L.-C., Larco, J. C., Carrera, E. V. & León, R. A deep learning approach for automatic recognition of seismo-volcanic events at the Cotopaxi volcano. *J. Volcanol. Geotherm. Res.* **409**, 107142 (2021).
12. Ma, Z. & Mei, G. Deep learning for geological hazards analysis: Data, models, applications, and opportunities. *Earth-Sci. Rev.* **223**, 103858 (2021).
13. Martínez, V. L. *et al.* Advanced signal recognition methods applied to seismo-volcanic events from Planchon Peteroa Volcanic Complex: Deep Neural Network classifier. *J. South Am. Earth Sci.* **107**, 103115 (2021).
14. Rey-Devesa, P. *et al.* Universal machine learning approach to volcanic eruption forecasting using seismic features. *Front. Earth Sci.* **12**, 1342468 (2024).
15. Salazar, A., Arroyo, R., Perez, N. & Benitez, D. Deep-Learning for Volcanic Seismic Events Classification. in *2020 IEEE Colombian Conference on Applications of*

Computational Intelligence (IEEE ColCACI 2020) 1–6 (IEEE, Cali, Colombia, 2020). doi:10.1109/ColCACI50549.2020.9247848.

16. Tan, D. *et al.* Detection and Characterization of Seismic and Acoustic Signals at Pavlof Volcano, Alaska, Using Deep Learning. *J. Geophys. Res. Solid Earth* **129**, e2024JB029194 (2024).
17. Titos, M., Bueno, A., Garcia, L. & Benitez, C. A Deep Neural Networks Approach to Automatic Recognition Systems for Volcano-Seismic Events. *IEEE J. Sel. Top. Appl. Earth Obs. Remote Sens.* **11**, 1533–1544 (2018).
18. Barberi, G. *et al.* La sismicità dell'area etnea nel periodo gennaio – dicembre 2020. *Quad. Geofis.* **179**, 1–30 (2022).
19. Ferrari, F. *et al.* La sismicità dell'area etnea nel periodo Gennaio – Dicembre 2021. *Quad. Geofis.* **192**, 1–32 (2024).
20. Andronico, D., Cannata, A., Di Grazia, G. & Ferrari, F. The 1986–2021 paroxysmal episodes at the summit craters of Mt. Etna: Insights into volcano dynamics and hazard. *Earth-Sci. Rev.* **220**, 103686 (2021).
21. Bennis, K. L. & Andrews, B. *Global Volcanism Program: Report on Etna (Italy).* https://volcano.si.edu/showreport.cfm?doi=10.5479/si.GVP.BGVN202308-211060 (2023).
22. Bean, C. J. *et al.* Long-period seismicity in the shallow volcanic edifice formed from slow-rupture earthquakes. *Nat. Geosci.* **7**, 71–75 (2014).
23. Matoza, R. S. & Roman, D. C. One hundred years of advances in volcano seismology and acoustics. *Bull. Volcanol.* **84**, 86 (2022).
24. Alparone, S., Andronico, D., Lodato, L. & Sgroi, T. Relationship between tremor and volcanic activity during the Southeast Crater eruption on Mount Etna in early 2000. *J. Geophys. Res. Solid Earth* **108**, 2002JB001866 (2003).
25. Cannata, A. *et al.* Space-Time Evolution of Magma Storage and Transfer at Mt. Etna Volcano (Italy): The 2015–2016 Reawakening of Voragine Crater. *Geochem. Geophys. Geosystems* **19**, 471–495 (2018).
26. Di Grazia, G. *et al.* A multiparameter approach to volcano monitoring based on 4D analyses of seismo-volcanic and acoustic signals: The 2008 Mt. Etna eruption. *Geophys. Res. Lett.* **36**, 2009GL039567 (2009).
27. Patanè, D. *et al.* Insights into magma and fluid transfer at Mount Etna by a multiparametric approach: A model of the events leading to the 2011 eruptive cycle. *J. Geophys. Res. Solid Earth* **118**, 3519–3539 (2013).
28. Sciotto, M., Cannata, A., Di Grazia, G. & Montalto, P. Volcanic tremor and long period events at Mt. Etna: Same mechanism at different rates or not? *Phys. Earth Planet. Inter.* **324**, 106850 (2022).
29. Cannata, A. *et al.* Monitoring Seismo-volcanic and Infrasonic Signals at Volcanoes: Mt. Etna Case Study. *Pure Appl. Geophys.* **170**, 1751–1771 (2013).
30. Sciotto, M., Cannata, A., Gresta, S., Privitera, E. & Spina, L. Seismic and infrasound signals at Mt. Etna: Modeling the North-East crater conduit and its relation with the 2008–2009 eruption feeding system. *J. Volcanol. Geotherm. Res.* **254**, 53–68 (2013).
31. Cannavò, F. *et al.* A multivariate probabilistic graphical model for real-time volcano monitoring on Mount Etna. *J. Geophys. Res. Solid Earth* **122**, 3480–3496 (2017).

32. Alparone, S. *et al.* Seismological constraints on the 2018 Mt. Etna (Italy) flank eruption and implications for the flank dynamics of the volcano. *Terra Nova* **32**, 334–344 (2020).
33. Corradino, C. *et al.* Mapping Recent Lava Flows at Mount Etna Using Multispectral Sentinel-2 Images and Machine Learning Techniques. *Remote Sens.* **11**, 1916 (2019).
34. Musu, A. *et al.* The magmatic evolution of South-East Crater (Mt. Etna) during the February–April 2021 sequence of lava fountains from a mineral chemistry perspective. *Bull. Volcanol.* **85**, 33 (2023).
35. Carleo, L., Currenti, G. & Bonaccorso, A. Clustering of eruptive events from high-precision strain signals recorded during the 2020–2022 lava fountains at the Etna volcano (Italy). *Nat. Hazards Earth Syst. Sci.* **23**, 1743–1754 (2023).
36. Nunnari, G. Clustering activity at Mt Etna based on volcanic tremor: A case study. *Earth Sci. Inform.* **14**, 1121–1143 (2021).
37. Spampinato, S., Langer, H., Messina, A. & Falsaperla, S. Short-term detection of volcanic unrest at Mt. Etna by means of a multi-station warning system. *Sci. Rep.* **9**, 6506 (2019).
38. Cannata, A., Sciotto, M., Spampinato, L. & Spina, L. Insights into explosive activity at closely-spaced eruptive vents using infrasound signals: Example of Mt. Etna 2008 eruption. *J. Volcanol. Geotherm. Res.* **208**, 1–11 (2011).
39. Eckel, F., Langer, H. & Sciotto, M. Monitoring sources of volcanic activity at Mount Etna using pattern recognition techniques on infrasound signals. *Geophys. J. Int.* **232**, 1–16 (2022).
40. Watson, L. M. Using unsupervised machine learning to identify changes in eruptive behavior at Mount Etna, Italy. *J. Volcanol. Geotherm. Res.* **405**, 107042 (2020).
41. Abazari, A., Hajian, A., Kimiaefar, R., Hodhodi, M. & Gambino, S. A deep learning approach to classify volcano activity using tremor data joint with infrasonic event counts and radar backscatter power: case study: mount Etna, Italy. *Acta Geophys.* **73**, 131–142 (2024).
42. Fee, D. *et al.* A generalized deep learning model to detect and classify volcano seismicity. *Volcanica* **8**, 305–323 (2025).
43. Zali, Z. *et al.* Low-frequency tremor-like episodes before the 2023 MW 7.8 Türkiye earthquake linked to cement quarrying. *Sci. Rep.* **15**, 6354 (2025).
44. Jenkins, W. F., Gerstoft, P., Bianco, M. J. & Bromirski, P. D. Unsupervised Deep Clustering of Seismic Data: Monitoring the Ross Ice Shelf, Antarctica. *J. Geophys. Res. Solid Earth* **126**, e2021JB021716 (2021).
45. Mousavi, S. M., Zhu, W., Ellsworth, W. & Beroza, G. Unsupervised Clustering of Seismic Signals Using Deep Convolutional Autoencoders. *IEEE Geosci. Remote Sens. Lett.* **16**, 1693–1697 (2019).
46. Snover, D., Johnson, C. W., Bianco, M. J. & Gerstoft, P. Deep Clustering to Identify Sources of Urban Seismic Noise in Long Beach, California. *Seismol. Res. Lett.* **92**, 1011–1022 (2021).
47. Giuffrida, M., Cardone, M., Zuccarello, F. & Viccaro, M. Etna 2011–2022: Discoveries from a decade of activity at the volcano. *Earth-Sci. Rev.* **245**, 104563 (2023).
48. Proietti, C., De Beni, E. & Cantarero, M. One hundred lava flows of Mt. Etna, Italy: July 2019–December 2023 update. *J. Maps* **20**, 2380899 (2024).

49. Moschella, S., Cannata, A., Di Grazia, G. & Gresta, S. Insights into lava fountain eruptions at Mt. Etna by improved source location of the volcanic tremor. *Ann Geophys* **61**, (2018).
50. Eibl, E. P. S. *et al.* Evolving shallow conduit revealed by tremor and vent activity observations during episodic lava fountaining of the 2021 Geldingadalir eruption, Iceland. *Bull. Volcanol.* **85**, 10 (2023).
51. Mousavi, S. M. & Beroza, G. C. Machine Learning in Earthquake Seismology. *Annu. Rev. Earth Planet. Sci.* **51**, 105–129 (2023).
52. Hinton, G. E. & Salakhutdinov, R. R. Reducing the Dimensionality of Data with Neural Networks. *Science* **313**, 504–507 (2006).
53. Cawley, G. C. & Talbot, N. L. C. On Over-fitting in Model Selection and Subsequent Selection Bias in Performance Evaluation. *J. Mach. Learn. Res.* **11**, 2079–2107 (2010).
54. Davies, D. L. & Bouldin, D. W. A Cluster Separation Measure. *IEEE Trans. Pattern Anal. Mach. Intell.* **PAMI-1**, 224–227 (1979).
55. Calinski, T. & Harabasz, J. A dendrite method for cluster analysis. *Commun. Stat. - Theory Methods* **3**, 1–27 (1974).
56. Cieslak, M. C., Castelfranco, A. M., Roncalli, V., Lenz, P. H. & Hartline, D. K. t-Distributed Stochastic Neighbor Embedding (t-SNE): A tool for eco-physiological transcriptomic analysis. *Mar. Genomics* **51**, 100723 (2020).
57. Van der Maaten, L. & Hinton, G. Visualizing Data using t-SNE. *J. Mach. Learn. Res.* **9**, 2579–2605 (2008).
58. De Beni, E. *et al.* The continuing story of Etna's New Southeast Crater (2012–2014): Evolution and volume calculations based on field surveys and aerophotogrammetry. *J. Volcanol. Geotherm. Res.* **303**, 175–186 (2015).
59. Barberi, G. *et al.* Mt. Etna Revised Seismic Catalog from 2020 (EtnaRSC2020). 500 MB Istituto Nazionale di Geofisica e Vulcanologia (INGV) https://doi.org/10.13127/ETNASC/ETNARSC2020 (2020).
60. Corsaro, R. A., Miraglia, L., Arienzo, I. & Di Renzo, V. The 2020–2022 paroxysmal episodes of the South-East Crater (Mt. Etna): insights into high-frequency eruptive activity from petrological monitoring. *Bull. Volcanol.* **86**, 85 (2024).
61. De Gori, P. *et al.* Re-pressurized magma at Mt. Etna, Italy, may feed eruptions for years. *Commun. Earth Environ.* **2**, 216 (2021).